Tortuosity in Variously-Structured Platelet Particles

Kyoka Ishiyama†, Keita Yamamoto†, Shusaku Harada†*, Tsubasa Yagi‡

† Division of Sustainable Resources Engineering, Faculty of Engineering, Hokkaido University, N13-W8, Sapporo, Hokkaido, 060-8628, Japan

‡ Radioactive Waste Management Funding and Research Center, 6-4, Akashicho, Chuo-ku, Tokyo, 104-0044, Japan

* Corresponding author: Shusaku Harada
Phone/Fax: + (81)-11-7066310
E-mail address: harada@eng.hokudai.ac.jp

ABSTRACT

Numerical investigations of pore characteristics in platelet particles with various macroscopic structures were performed for fundamental understanding of transport properties in clay layers composed of montmorillonite particles. The effect of macroscopic structures of particles on the geometric characteristics of pore networks were examined, particularly focusing on the tortuosity which represents the sinuosity of voids. Monte Carlo simulations of platelet particles under various initial configurations were performed to obtain metastable structures with internal differences. A random walk analysis was performed in extracted macropores of platelet structures. The tortuosity of pore network in variously-structured platelet particles was evaluated from the results of the random walk analysis. The numerical results showed that the macrostructures of particles form complicated pore networks, which significantly influence the tortuosity. The "diffusional" tortuosity obtained from the random walk analyses was compared with the existing "geometrical" tortuosity model. It was found that configurational characteristics of platelets, such as size and orientation angle of particle clusters, was vital to estimate the tortuosity. The obtained tortuosity was also compared with the experimental results of the diffusion coefficient in clay layers obtained from previous studies. The results suggested that a complicated density dependence of diffusivity in clay arises from the diversity of macroscopic particle structures.

Key words: tortuosity, platelet particles, macroscopic structures, diffusivity

1. Introduction

Transport phenomena in porous media is important for many processes in various engineering fields, such as dispersion process of contamination in soil (Patil and Chore, 2014), engineered barrier systems of repositories in TRU (Trans-Uranic) waste disposal process (Åkesson, et al., 2010) and so on. Many previous studies have shown that such transport properties are not simply dependent on porosity alone, but are affected by various geometric characteristics of pores. For example, the fluid permeability in porous media has been modeled as functions of the porosity, the specific surface area and the tortuosity (Carman, 1937). In some cases, the diffusivity has been expressed by the tortuosity and the constrictivity of pores (Holzer, et al., 2013, Keller, et al., 2015). These pore characteristics vary significantly depending on the structure of media, for example, the particle size distribution or packing structure in case of particulate beds.

Among the pore characteristics listed above, this study focuses on tortuosity, a crucial parameter for quantifying pore sinuosity and complexity. As will be discussed later, the tortuosity in porous media is variously defined in different fields, such as "geometrical" tortuosity, "diffusional" tortuosity, and so on (Clennell, 1997). There have been various discussions on the validity of existing models and the compatibility of different definitions of tortuosity (Ghanbarian et al. 2013), and in recent years, there have been attempts to relate one definition of tortuosity to another (Fu et al. 2021).

In porous media composed of solid particles, the particle shape also influences macropore characteristics including the tortuosity. For example, spherical particle layers have little variation in pore sinuosity. For this reason, the tortuosity has been modeled as a simple function of porosity (or apparent density) alone (Millington, 1959; Weissberg, 1963; Boudreau, 1996; Koponen et al., 1996; Ahmadi et al., 2011). However, layers of anisotropic particles such as platelets and rods, contain highly complex packing configurations, and consequently internal pore characteristics are also complicated. Therefore, the tortuosity is not determined by the porosity alone. Accordingly, it is crucial to account for macroscopic structural properties such as clustering features, when estimating the tortuosity in anisotropic particle layers. For example, Daigle and Dugan (2011) established the tortuosity model in a cylinder-shaped particle bed, which assumed assemblies of platelet clusters, and showed that the tortuosity greatly depends on the size and the orientation angle of clusters. Although the validity of their model has not been fully verified, it illustrates the importance of particle macrostructures for predicting the tortuosity.

Tortuosity in platelet structures is closely related to mass transfer in clay layers, which is important in TRU waste disposal processes as stated above. Clay particles are well-known to typically exhibit thin sheet-like shapes, and therefore they are often modeled as platelets in the structural analyses (Dijikstra et al., 1997). Furthermore, as mentioned above, the tortuosity is related to the diffusivity in the media, so that evaluating tortuosity in platelet structures aids in understanding the diffusivity in clay layers. For example, Keller et al. (2011) discussed the diffusion anisotropy in clay layers by examining the anisotropy of the tortuosity. They constructed a three-dimensional network of flow-contributing voids in clay layers and quantified the vertical and horizontal tortuosities.

To evaluate the tortuosity in clay, it is important to understand the relation of the macrostructures of particles to macropores in clay layers. Previous studies have shown that in nature, smectite-type clays form clusters of several particles (Wong and Wang, 1997). Such clustering of particles may bring heterogeneity in pore size, anisotropy in the flow path (Olsen, 1962), and dead-end pores (Hong, 2020), leading to complicated pore networks. In an attempt to assess how such intricate void structures influence the transport properties, Bacle et al. (2016) simulated various platelet structures and investigated the effects of structural differences on the diffusivity. They applied the Gay-Berne potential to platelets assumed to represent clays and estimated the diffusivity in macropores, but the validity of their analysis is unclear because their model allowed particles to overlap.

Further caution is needed to assess how pore networks facilitate mass transfer in clay layers containing particle clusters. In general, the width of interlayer spaces in clay clusters are on the nanometer scale, and it is unclear how such tiny gaps contribute to overall mass transport. For example, Bacle et al. (2016) analyzed the diffusion coefficient in platelet bed and noted that diffusivity within particle clusters is smaller than outside. Boţan et al. (2011) performed molecular simulations assuming electrical interaction between clay particle surfaces and water molecules. They found that fluids cannot be regarded as a continuum in pores smaller than a few nanometers. There is thus evidence that transport phenomena in nanopores contrast with those in outer macropores and they might be treated differently. For example, Wong and Wang (1997) reported limited water flow through tiny pores in particle clusters that cannot be driven by the hydraulic gradient. In another example, Li et al. (2018) separated voids into inner pores (micropores in particle clusters) and outer pores (macropores between clusters). They evaluated the permeability in clays based on the outer pore characteristics alone, assuming that the mass transfer in inner pores was negligible.

If only outer pores affect mass transfer, as reported in previous studies, it is important to quantify geometric characteristics of macrostructures of particles, which influences macropore characteristics. Li et al. (2018) examined the aspect ratio and the orientation angle of particle clusters from existing experimental results in clay layers, which were estimated to be approximately 2 to 3 and 30 to 60 degrees, respectively. Adams et al. (2013) observed resedimented clay structures with BSEM (Backscattered Scanning Electron Microscope). The two-dimensional assessment revealed that the aspect ratio of particle cluster was approximately 2 and the orientation angle was 30 to 50 degrees, respectively. However, the structure of clay particles depends on their formation processes, it is possible for various configurations to result even at a given density. Therefore, it is difficult to generalize the type of macroscopic structures in clay layers and their internal pore network.

In this study, various structures of platelet particles, particularly clustered and almost-stacked structures (e.g. Schneider et al., 2011), were simulated under simple assumptions to investigate the macropore characteristics in particle layers. The tortuosity in these structures was calculated from a random walk analysis. Furthermore, in comparison with the existing geometrical tortuosity model, the compatibility of differently-defined tortuosities and the applicability of the model were examined. Finally, the relationship between the diffusional tortuosity and macroscopic structures of clay particles were investigated by comparing the results with diffusion experiments in clay layers under specific density conditions, to gain physical insights of complicated diffusivity in clay, which has been reported in previous studies.

2. Numerical Method

2.1 Monte Carlo Analysis

In order to evaluate pore characteristics in clay layers, the internal structure, i.e., the arrangement of clay particle have to be considered. However, details of actual clay structures have not been fully understood. Therefore, this study modeled clay particles as platelets and computed various particle structures with different density conditions using a Monte Carlo analysis, which was used to investigate the relationship between macroscopic particle structures and pore networks. In this section, the simulation method of platelet structures conducted in this study is described below.

Bentonite clays are mainly composed of montmorillonite particles that have charged surfaces. A number of analyses of clay structure have been performed to explore the interaction between such particles. For example, Dijkstra et al. (1997) performed structural analysis that assumed a quadrupole potential for infinitely thin platelets. They reported that platelets at low densities exhibited edge-to-face configurations and were locally aggregated into "house-of-cards" structures, similar to those observed in actual clay particles. In contrast, increasing density results in structures that approached a nematic state with a parallel platelet arrangement. However, there may be thought practical limits to calculations that assume certain electrical interactions in higher density conditions. Bacle et al. (2016) applied the Gay-Berne potential to platelets with a finite thickness. They calculated the high-density structures allowing for overlap of particles. Terada et al. (2018) performed a structural analysis by assuming the rigid-body potential on infinitely thin platelets and examined the consistency with those using a quadrupole potential at moderate to high density. As the density increased, nematic structures were confirmed to occur due to stacking of platelets by excluded volume effects. Their results suggested that the rigid-body potential would be applicable at high-density conditions.

In order to examine how macroscopic structures affect pore characteristics, a structural analysis of platelet particles was performed using a Monte Carlo method. The details of the analyses is similar to those by Terada et al. (2018). The calculation methods for various structures at given density are described later. The rigid body potential was applied to infinitely thin platelets with diameter σ. The cubic calculation region was considered and periodic boundary conditions were applied in all directions. The size of the calculation region was chosen to be sufficiently large relative to the structural formations, with an edge size L that was four times larger than the particle diameter σ. By setting the number of platelets N = 1920, 3200, 4480, 6400, 9600 and 10880, the analyses were performed using values of the non-dimensional density $N\sigma^3/L^3$ ranging from 30 to 170. To calculate the dry density, the platelet was assumed to be monodisperse montmorillonite with a diameter σ= 320 nm, a thickness d = 1 nm and a density ρ =2.7 Mg/m^3. The corresponding dry density conditions $\rho_d = \rho\pi\sigma^2 dN/4L^3$ are ranging from 0.20 to 1.13 Mg/m^3. In general, the range of dry densities of clays is considered from 0.2 Mg/m^3 to 2.0 Mg/m^3. There are two reasons why the analyses were performed only for low to moderate density conditions. The first reason is that the Monte Carlo simulation at large density takes an enormous computation time, since the present analysis does not allow overlapping of particles. The second is that it is difficult to form different macrostructures of platelet particles, because the number of possible configuration states of particle is very few at large densities (>1.0 Mg/m^3) by excluded volume effect. However, the present analysis captures the discontinuous change of pore characteristics of platelet layers with the density increase, as described later.

The initial state was made by randomly generated platelet positions and normal vectors. Geometric calculations were used to verify the intersections of each particle to avoid overlap. The position and orientation of each particle were then updated by random numbers, and the post-transition state was determined based on the Metropolis method. In this step, particle intersection was checked to avoid overlap. The maximum movement per translation was set to $\Delta r = 0.02\sigma$ and the maximum variation for each normal vector component was $\Delta v = 0.02$.

In this study, diverse structures under conditions of a given density were fabricated. Monte Carlo analysis is generally used to determine thermodynamic equilibrium states, so that even in simulations with different initial platelet arrangements, they should in principle converge to a single equilibrium state. In practice, Terada et al. (2018) performed structural analyses at various density conditions and calculated a single equilibrium structure for each condition. However, structures that vary from the equilibrium states may form, depending on the number of particles and the initial configurations. Therefore, various metastable structures were computed in this study, in which configurational changes became minute when calculating equilibrium states. Fig.1 shows examples of metastable structures of platelet system. 3D snapshots and cross-sectional views of platelet with different initial conditions at the same density are shown in Figs. 1(a) and (c). The Monte Carlo analysis conducted from these initial states yielded metastable structures, particularly clustered and almost-stacked structures (e.g. Schneider et al., 2011), which are shown in Figs. 1 (b) and (d).

In Fig. 1 (a), platelet angles were randomly assigned with the maximum angle θ_{ini} =84.3 degree (cos θ_{ini} =0.1) from the vertical direction in the initial state. Under these conditions, the platelets may be random at first, but random placement is significantly restricted when the number of platelets increases as much as excluded volume of each particle overlaps. Consequently, the particles are repositioned along with other platelets without assuming any specific potential. When the Monte Carlo simulation was started from these initial conditions, each particle moves seeking to increase the number of possible states at first, but the structures cease to change after plenty of Monte Carlo steps (Fig. 1b). That is, the structures other than the equilibrium states may form during the computation process depending on initial configurations. Such states are considered as metastable structures and they are defined as one with sufficiently little configurational change after a sufficient number of steps. Fig. 1(c) shows the initial platelet structure in which the initial orientation limiting angle was θ_{ini} =25.8 degree (cos θ_{ini} =0.9). Calculations starting from this state produced a metastable structure with laminated platelets (Fig. 1d). It is an entirely distinct structure compared to that shown in Fig.1(b), although they are the same density conditions. In this way, platelet structures with different internal configurations were fabricated.

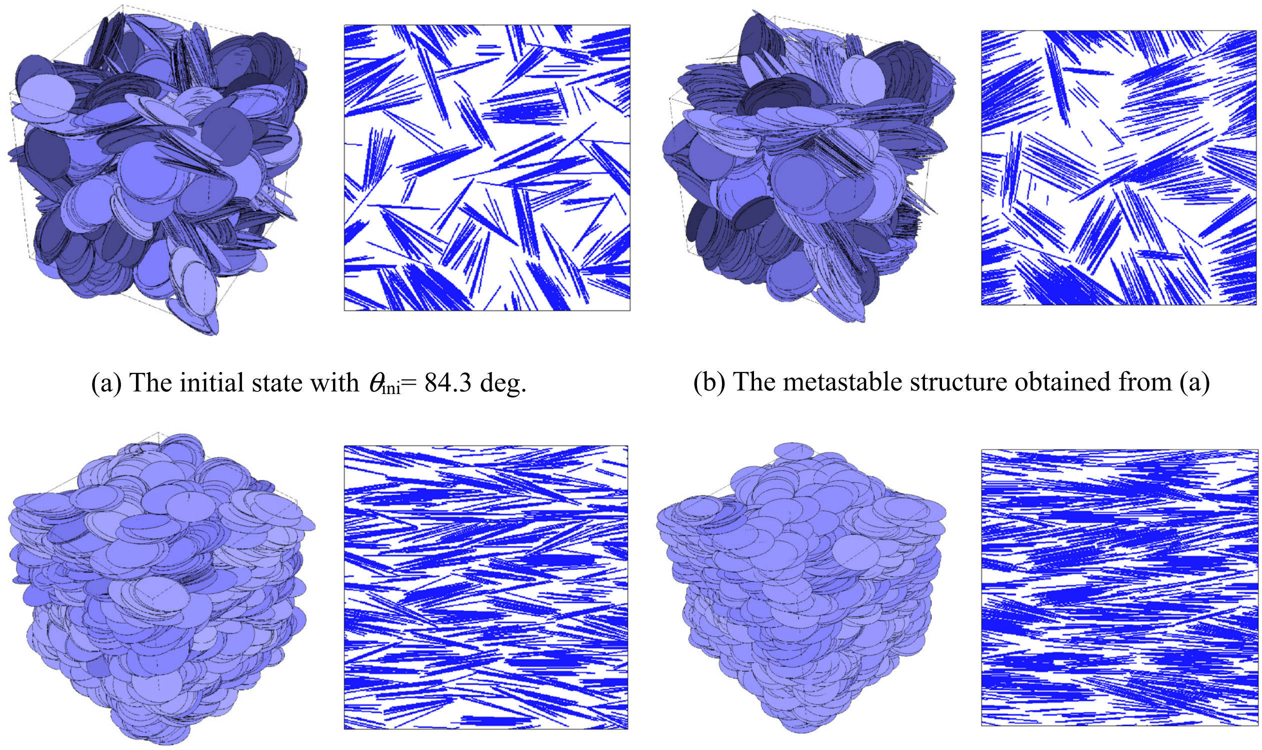

(a) The initial state with θ_{ini}= 84.3 deg. (b) The metastable structure obtained from (a)

(c) The initial state with θ_{ini}= 25.8 deg. (d) The metastable structure obtained from (c)

Fig. 1 3D snapshots and cross-sectional views of initial and metastable structures at a dry density of 0.33 Mg/m^3.

2.2 Extraction of Macropores

This study examined the influence of platelet structures on the macropore contributions to mass transport. As mentioned above, it is known that clay particles form clusters in nature. To capture the features of the macropores in such clusterized platelet structures, it is essential to investigate whether nanometer-sized micropores within particle clusters influence the overall mass transfer.

In previous studies, Wong and Wang (1997) distinguished water in clay layers as free water or intra-cluster water, where the former was present in macropores and could move along hydraulic gradients, whereas the latter occurred within particle clusters, and had restricted flow. Similarly, Li et al. (2018) separated the inner pores (inside particle clusters) from external pores and they categorized inner pores as solid phases and estimated the clay permeability solely from external pores. Nevertheless, it is challenging to precisely distinguish such pore types in clays. For example, mass transfer may differ depending on the width of the flow path and the size of molecules, with molecules behaving individually or collectively, similarly to the Knudsen flow for gases. In terms of pore networks, it is also unclear whether molecules in dead-end pores affect the overall mass transfer or fluid permeability (Hong, 2020). In addition, electrical interaction problems may arise from the formation of immobile water layers (Singh and Wallender, 2008) that can impede the motion of molecules. Thus, it is difficult to estimate the distinguished pores that contribute to transport phenomena from those that do not.

To provide a clue to these issues, Boţan et al. (2011) numerically evaluated the width of flow paths in which fluids can be regarded as continuous. Specifically, they performed molecular dynamics simulations of water in clay nanopores in which electrical interactions were assumed and presented the results of fluid velocity and viscosity for various micropore widths. They concluded that fluids could be regarded as continuous for pore widths of 3 nm or more if slip boundary conditions were assumed. However, the velocity distribution results indicated that Poiseuille flow disturbed near the surface even for pore widths of 6 nm. These findings suggest that 3 nm to 6 nm may be the minimum pore width for a fluid continuum.

Like previous studies, this study assumed that nanometer-sized micropores do not contribute to transport phenomena in the context of continuous transfer. However, as described above, it is not easy to distinguish between inner and outer pores strictly based on physical evidence. For this reason, the analysis in this study did not classify inner and outer pores and extracted macropores by void size only. Specifically, we conducted a local averaging procedure that “filled” the space of a few nanometers from the particle surfaces to obtain macropores. The filling width was approximately 3 to 6 nm, based on the results by Boţan et al. (2011). The detailed procedures are described as follows.

Macropores in a metastable platelet structure obtained by a Monte Carlo analysis were sterically isolated. First, the cubic calculation region was divided into 400×400×400 elements and a particle existence function $\rho(x, y, z)$ (= 0 or 1) was mapped for each voxel. Next, a local averaging was performed on the particle existence function to calculate the continuous particle concentration fields. This operation excludes tiny pores between platelets that do not contribute to mass transfer. In this study, the following three-dimensional Gaussian function was used as a weight function of the local averaging:

$$g(x,y,z)=\frac{1}{\left(2\pi\lambda^2\right)^{\frac{3}{2}}}\exp\left(-\frac{x^2+y^2+z^2}{2\lambda^2}\right) \tag{1}$$

where λ is the deviation parameter that determines the extent of the local averaging. Using Eq. (1), the particle concentration fields $c(x, y, z)$ were calculated as follows:

$$c(x,y,z)=\int_{-\infty}^{\infty} g(x-x',y-y',z-z')\rho(x',y',z')dx'dy'dz' \tag{2}$$

The kernel size of each voxel was 5×5×5, and voxels with particle concentrations of less than 0.001 were regarded as voids. Figure 2 shows the calculation results of the local-averaged particle concentration field along with some values of the deviation parameter λ. The black areas represent voids while the bright areas are solid phases. For a small λ value (Fig. 2a), each platelet existed individually with tiny pores present between particles. However, large λ values (Fig. 2c) "filled" the spaces between particle layers to eliminate micropores. Thus, the parameter selection is significant because the voids extracted from the results differ substantially. In this study, an optimal deviation parameter was decided as $\lambda = 0.003$, which corresponds to the extraction of micropores with a width of 3 nm to 6 nm. By the local averaging, micropores in particle clusters was filled, consistent with previous studies that assumed that interlayer pores do not contribute to mass transfer in clays (Wong and Wang, 1997; Li et al., 2018). It is noted that the exclusion of micropore does not result in the fragmentation of macropores, as described later.

(a) λ=0.001 (b) λ=0.005 (c) λ=0.01

Fig. 2 Particle concentration fields of metastable structure after local averaging with various deviation parameters λ.

2.3 Random Walk Analysis

In order to characterize the pores in terms of tortuosity, random walk analyses for various metastable structures were performed. The tortuosity represents the sinuosity and complexity of voids and has been previously used in various engineering fields. Intuitively, the tortuosity is expressed as the ratio of the pore channel length L_e to the length L along the flow direction in porous media. While "hydrological" tortuosity was originally introduced to describe fluid permeation (Carman, 1937), tortuosities with different definitions have been used when evaluating other transport properties (Clennell, 1997). For example, "diffusional" tortuosity (Satterfield and Sherwood, 1963), which is related to molecular diffusion, "electrical" tortuosity (Tye, 1983), which describes electrical conduction, and "geometrical" tortuosity (Adler, 1992), which characterizes the microstructure of porous media, have been defined. The compatibility of these tortuosities has not been well understood. Ghanbarian et al. (2013), for example, reviewed existing models and their compatibility of differently-defined tortuosities. Fu et al. (2021) classified various types of tortuosities into physical and geometrical ones. The former describes different transport processes in porous media, including hydraulic, electrical, diffusional, and thermal tortuosity, while the latter characterizes the morphological properties of pore structures. They investigated the compatibility of such properties in sandstones composed of isotropic particles. The results suggested differences between physical and geometrical tortuosities, and in some cases, a comparison among physical tortuosities may even reveal different values. In addition, the tortuosity of particle layers is highly dependent on the microstructure, such as the size, shape, orientation, and spatial distribution of particles and voids (Vervoort and Cattle, 2003), and the results may differ significantly depending on the system under investigation.

In this study, the "diffusional" tortuosity in platelet layers in the compaction direction was calculated from the results of random walk analyses. In general, diffusion in porous media, such as rocks and clays, is strongly influenced by complicated geometric void structures, such as porosity and tortuosity. The relationship between the apparent diffusion coefficient D_a in a porous medium and the self-diffusion coefficient D_0 in free water was proposed (García-Gutiérrez, 2004):

$$D_a = \frac{\phi}{\phi + \rho_d K_d} \frac{\delta}{\tau_d^{\,2}} D_0 \tag{3}$$

where ϕ is the porosity, ρ_d is the dry density, K_d is the distribution coefficient, δ is the constrictivity, and τ_d is the diffusional tortuosity. The constrictivity is a parameter that characterizes the so-called bottleneck effect in porous media (Holzer et al. 2013; Keller et al. 2015). As indicated in Eq.(3), the diffusion coefficient is a linear function of the constrictivity, while it is inversely proportional to the square of the tortuosity. In this study, δ was simply assumed to be 1, because the tortuosity shows a large value in the platelet system, as described later. Furthermore, in the case of non-sorbing diffusion, K_d can be regarded as 0. Therefore, the apparent diffusion coefficient D_a and the self-diffusion coefficient D_0 can be represented using the diffusional tortuosity τ_d as follows:

$$\frac{D_a}{D_0} = \frac{1}{\tau_d^{\,2}} \tag{4}$$

In general, molecular diffusion is governed by the Langevin equation or the Fokker-Planck equation and is sometimes analyzed using a random walk model, in which the mean-square displacement of many walkers at the long-time limit is proportional to the number of time steps. random walk analyses in macropores in platelet layers were calculated to statistically calculate the diffusion coefficient and the tortuosity via Eq. (4). The analyses were performed by similar method to Fu et al. (2021). The first step is to randomly place several walkers in voids at the initial state (t = 0). Then the walker positions are updated to selected neighboring voxels by random numbers. The walker position remains constant if the selected voxel is a solid phase. Repeating these steps yields the mean-square displacement with increasing time steps. Fu et al. (2021) computed the tortuosity of pores in sandstones in all x, y, and z directions. Such calculations are practical for isotropic systems with relatively straight flow paths, however, platelet structures have large bending channels and consequently the tortuosity varies greatly depending on the direction. The tortuosity was calculated from the mean-square displacement of walkers (from bottom to the top of Fig. 3). The mean-square displacement in z direction in free space where all regions are voids can be expressed as follows:

$$\left\langle z^2(t) \right\rangle_{\text{free}} = \frac{1}{N}\sum_{i=1}^{N}\left[z_i(t) - z_i(0) \right]^2 \tag{5}$$

where N is the number of random walkers, $z_i(t)$ is the position of the i-th walker at a given time, and $\langle\ \rangle$ represents the ensemble average. The self-diffusion coefficient D_0 can be calculated from the mean-square displacement by the following equation.

$$D_0 = \frac{1}{2}\frac{\left\langle z^2(t) \right\rangle_{\text{free}}}{dt} \tag{6}$$

Similarly, for random walkers in pore spaces, the mean square displacement in z direction (compaction direction of platelets) and the apparent diffusion coefficient D_a can be expressed as follows:

$$\left\langle z^2(t) \right\rangle_{\text{pore}} = \frac{1}{N}\sum_{i=1}^{N}\left[z_i(t) - z_i(0) \right]^2 \tag{7}$$

$$D_a = \frac{1}{2}\frac{\left\langle z^2(t) \right\rangle_{\text{pore}}}{dt} \tag{8}$$

The diffusional tortuosity τ_{dz} in z direction can be expressed from these ratios using Eqs. (6) and (8).

$$\tau_{dz} = \sqrt{\frac{D_0}{D_a}} = \sqrt{\frac{d\left\langle z^2(t) \right\rangle_{\text{free}} / dt}{d\left\langle z^2(t) \right\rangle_{\text{pore}} / dt}} \tag{9}$$

The calculation was performed over 10,000,000 time steps with 10,000 random walkers. Periodic boundary conditions were applied in the analysis. Figure 3 indicates the trajectories of three random walkers over 500,000 time steps as examples. The positions at each of the 500,000 time steps are shown as spheres connected by lines. At first glance, the three trajectories appear to be disconnected, but in fact they are all connected. This is because the trajectories that cross periodic boundaries are not connected by lines for the sake of clarity. Therefore the trajectories of walkers moving back and forth near the periodic boundary appear to be isolated.

As can be seen in Fig. 3 (a), walkers move between clustered platelets at random. This indicates that the relatively large macropores between clusters, which can be visually confirmed, are connected

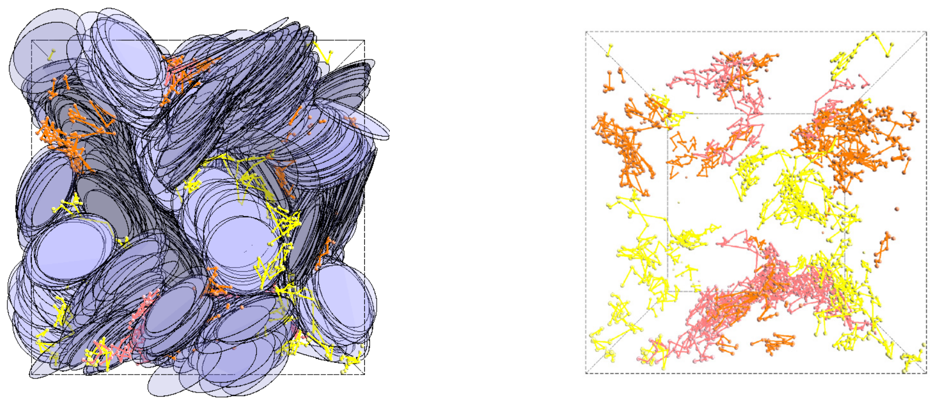

(a) viewpoint #1

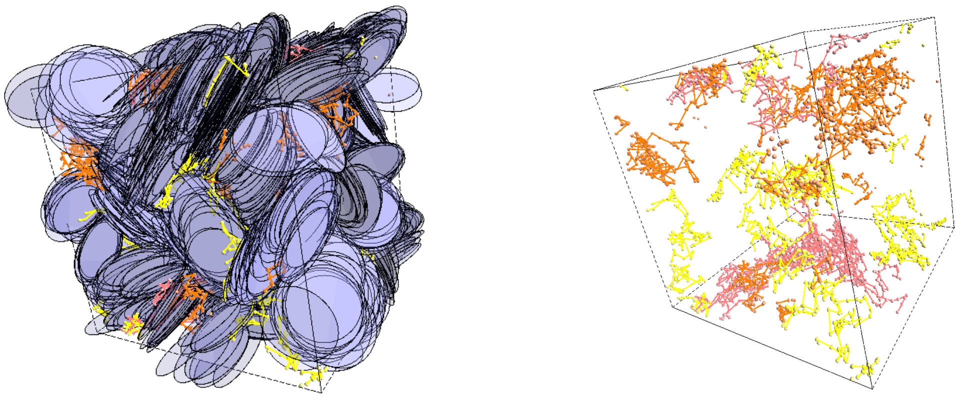

(b) viewpoint #2

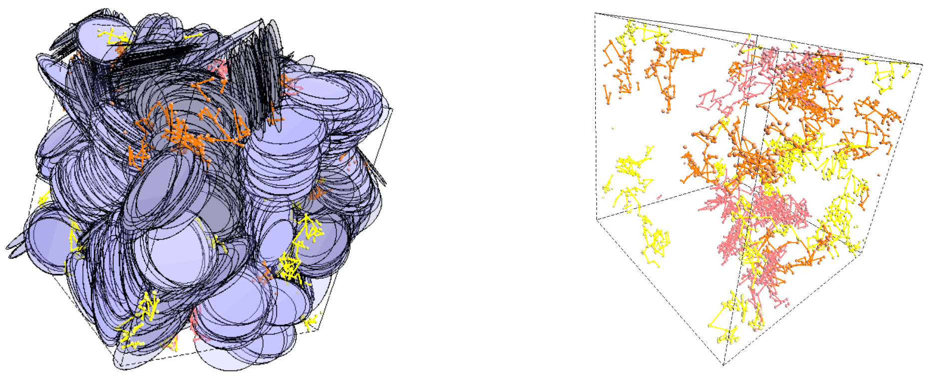

(c) viewpoint #3

Fig. 3 Random walker trajectories observed from different viewpoints; (left) overview, (right) trajectories. Trajectories of three walkers are indicated as examples. For the sake of clarity, trajectories that cross periodic boundaries are not connected by lines.

in three dimensions, allowing walkers to pass through them sufficiently. From checking the walker trajectories, it was confirmed that macropore is not fragmented by the exclusion of micropores in the process of the local averaging. In order to recognize the trajectory easily,Fig.3(b) shows the trajectories of three random walkers without indication of platelets. As shown in Fig.3 (b), there was sufficient movement in the computational domain even during 500,000 time steps.

2.4 Cluster Judgement

Because macroscopic configurations of clay particles are highly complicated and often unclear, various efforts have been made to quantitatively evaluate clay structures. Adams et al. (2013) conducted BSEM characterization of resedimented mudstones to estimate particle structures from image analysis. Their two-dimensional evaluations found a particle cluster aspect ratio of approximately 2 with orientation angles of approximately 30 to 50 degrees. Li et al. (2018) developed a theoretical model relating the angle and size of particle clusters to evaluate permeability in a smectite mudstone. Based on the previous study of clay swelling (Wong and Wang, 1997), they constructed a model relating particle angles to porosity and applied their model to mudstones used in previous studies (Gautam, 2004; Chalindar, 2010; Schneider et al., 2011), for which they obtained the angle and aspect ratio of particle clusters. According to the summarized data, the orientation angle of the smectite mudstone was approximately 30 to 60 degrees with a cluster aspect ratio around 2 to 3. Although the validity of these values still needs to be verified, it underscores the importance of knowing the size and configuration of clusters in order to estimate particle structures in clay quantitatively.

In order to evaluate the shape and size of particle clusters in the metastable structures obtained by Monte Carlo analysis quantitatively, a cluster judgment of platelets was performed. This judgment determined the clusters to which each platelet belonged, using procedures similar to those by Wouterse et al. (2007). Firstly, candidate particles that could form the center of each cluster were identified. The location vectors of particles *i* and *j* are $\boldsymbol{r}_i$ and $\boldsymbol{r}_j$, and the normal vectors are $\boldsymbol{u}_i$ and $\boldsymbol{u}_j$, respectively. The correlation of the normal vector with adjacent particles at each particle location was then calculated using a normalized Gaussian function as follows:

$$c(\boldsymbol{r}_i) = \sum_{j \neq i}^{N} \exp\left[-\frac{(\boldsymbol{r}_i - \boldsymbol{r}_j)^2}{2\alpha^2} \right] (\boldsymbol{u}_i \cdot \boldsymbol{u}_j) \tag{10}$$

where α is the spread of correlation. The particles were then sorted at the highest $C(\boldsymbol{r}_i)$ value, selecting higher particles as candidates for the center of each cluster. Furthermore, we verified whether the particle orientation was aligned from Eq. (11), whether the normal distance between particles was close using Eq. (12), and whether the tangential distance between particles was small using Eq. (13) for candidate particles and adjacent particles:

$$\left|\boldsymbol{u}_i \cdot \boldsymbol{u}_j\right| > 1 - \delta_{pc} \tag{11}$$

$$\left|(\boldsymbol{r}_i - \boldsymbol{r}_j) \cdot \boldsymbol{u}_j\right| < \delta_{nc} \tag{12}$$

$$\frac{1}{2}\left|(\boldsymbol{r}_i - \boldsymbol{r}_j) - (\boldsymbol{r}_i - \boldsymbol{r}_j) \cdot \boldsymbol{u}_i \boldsymbol{u}_i\right| + \frac{1}{2}\left|(\boldsymbol{r}_i - \boldsymbol{r}_j) - (\boldsymbol{r}_i - \boldsymbol{r}_j) \cdot \boldsymbol{u}_j \boldsymbol{u}_j\right| < \delta_{sc} \tag{13}$$

where δ_{pc}, δ_{nc}, and δ_{sc} are the cluster judgment parameters and $\delta_{pc} = 0.06$, $0.075\sigma < \delta_{nc} < 1.0\sigma$, and $0.2\sigma < \delta_{sc} < 0.25\sigma$, respectively ($\sigma$: platelet diameter). Figure 4 shows an example of the cluster judgment results for a metastable structure at a dry density of 0.33 Mg/m^3. In the figure, platelet particles identified as the same cluster are shown in identical colors and isolated platelets are shown in black. As shown in Fig.4, clusters of different size and orientation can be observed in a single platelet structure. These cluster characterizations make it possible not only to clearly visualize the structural properties but also to quantitatively estimated of cluster geometric properties such as the aspect ratio. The details of the calculation method for the aspect ratio is described below.

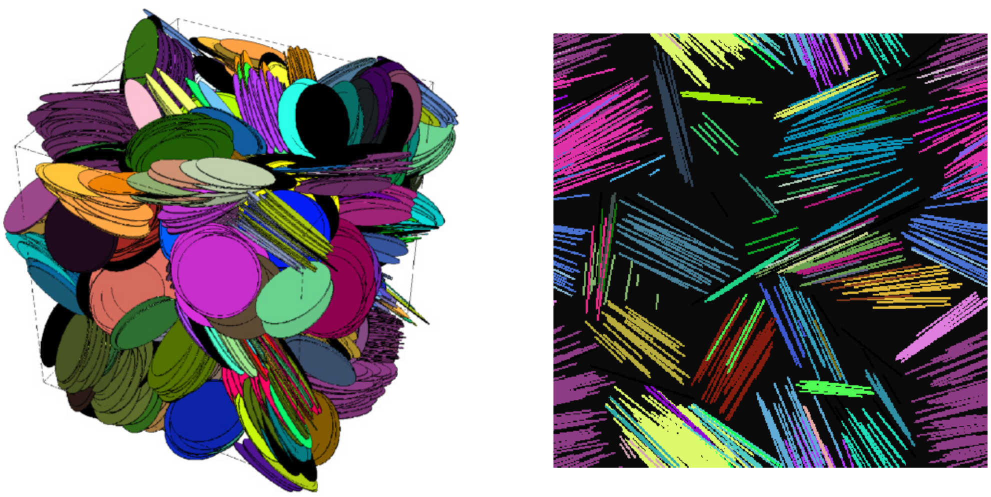

(a) 3D snapshot (b) cross-sectional view

Fig. 4 Cluster judgement for metastable structure at dry density 0.33 Mg/m^3.

3. Results and Discussion

3.1 Platelet Structures from Monte Carlo Analysis

This aim of this study is to investigate the influence of platelet configurations on pore networks and their contribution to mass transfer. In order to obtain metastable structures with differing internal geometries, Monte Carlo analyses were performed under various initial conditions. Then macropores in the platelet structures were isolated by local averaging procedures. Figure 5 shows partial cross-sectional views of macropores (white part) and solid phase with micropore (blue part) for various platelet structures (dry density from 0.20 to 1.13 Mg/m^3). As seen in the figure, various platelet structures are fabricated even at the same dry density by the Monte Carlo analyses with different initial configurations. If the initial orientation angle of the platelets is large, only a few possible particle states exist at a high density and a considerable amount of time is required to randomly arrange the particles. Accordingly, only a stacked structure is shown for conditions with dry densities greater than 0.99 Mg/m^3 in Fig.5.

The characteristics of the solid phases with micropores (blue part) reveal that the size and angle of platelet clusters are entirely different for the various initial states at each density condition. For example, when the initial orientation angle limit was large, platelets became aggregated into clusters of various sizes and angles, while smaller initial angles produced flat clusters with aligned orientations. Of course, it is unknown which structures are similar to those of actual clay layers at this stage. Concerning macropores (white part), large voids are connected between clusters in the structures containing large-angled clusters (upper column), constituting pore networks that extend in various directions. Although the macropores appear to be partially isolated in the 2D cross-sectional view, the random walk analysis confirmed that they are connected in 3D. In the structures with small-angled clusters (lower column), tiny voids are connected along the lamination direction of the platelets and pore networks exhibit significant anisotropy.

The discussion given here highlights how remarkably different pore characteristics can develop depending on the macroscopic structural properties of particles, such as size and orientation of.

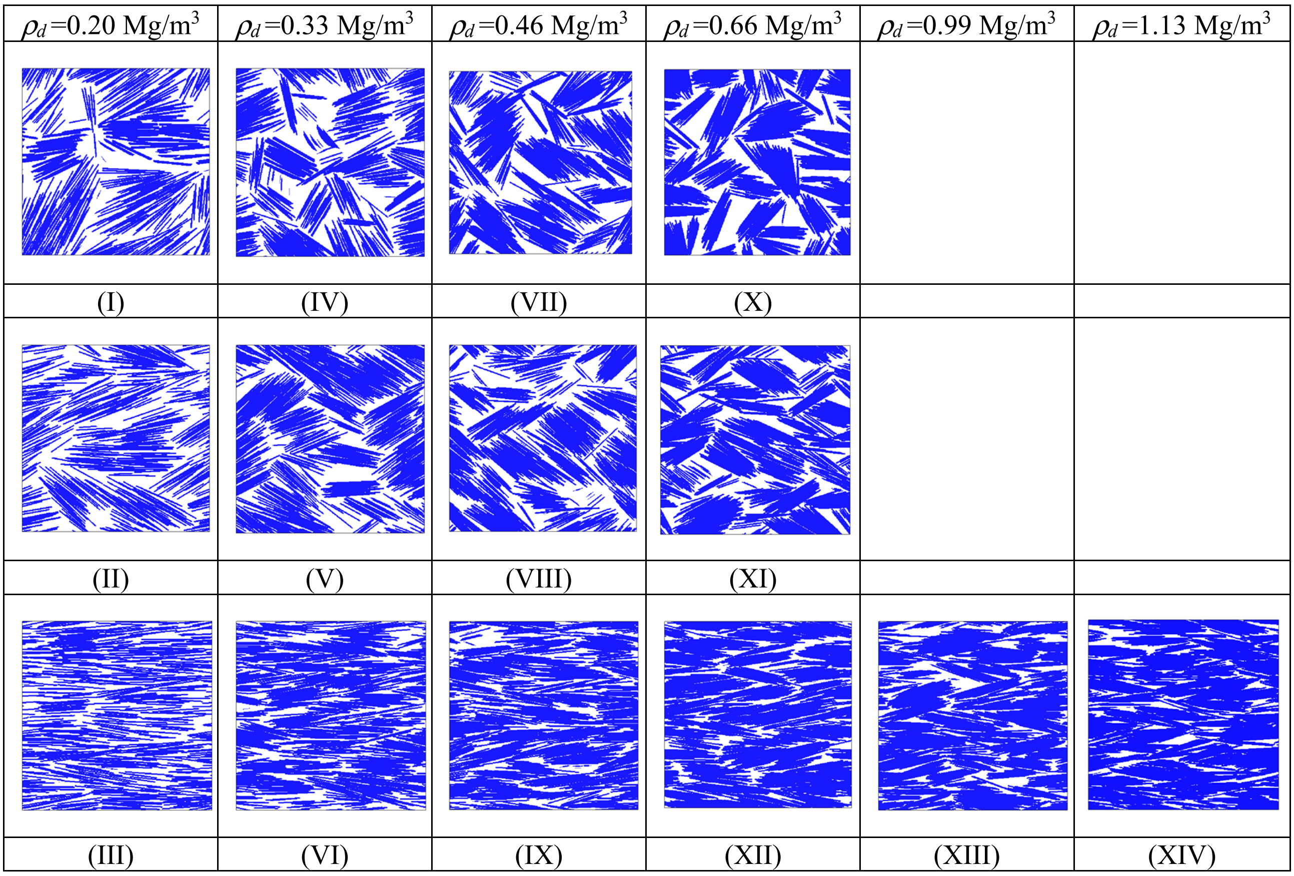

Fig. 5 Results of extraction of macropores in metastable structures at various density conditions. The white part represents macropores and the blue part is solid phase with micropores. The initial orientation limiting angle θ_{ini} =84.3 deg. (upper), 60.0 deg. (middle) and 25.8 deg. (lower), respectively.

clusters These results may significantly influence the tortuosity which represents the sinuosity and complexity of voids. The above results implies the importance of knowing the macroscopic internal structures, including macropores, on estimating transport properties in clay layers. It should be noted again that, it is not clear which platelet structure represents actual clay layers because the macrostructures of clay are still unspecified at respective density conditions.

3.2. Tortuosity from Random Walk Analysis

Considering that the pore characteristics are affected by macrostructural differences within platelet structures, the tortuosity also varies with the internal structure under the same density conditions. In this section, the relationship between the tortuosity from a random walk analysis and the platelet structure is discussed. The mean-square displacements of walkers in one direction (z direction) were computed from a three-dimensional random walk simulation both in macropores of platelet structures and free space. The tortuosity can be obtained by substituting these results into Eq. (9). It corresponds to "diffusional" tortuosity among various definitions of tortuosity as described above.

Table 1 shows the diffusional tortuosity in the z direction τ_{dz} determined by a random walk simulation. The roman numerals in the table correspond to the metastable structure numbers (see Fig. 5). The effective porosity ϕ_e, the average orientation angle θ_{fa}, and the aspect ratio of the particle clusters m_{eq} for each platelet structure are also summarized. These values are needed to compare the results with the existing tortuosity model, as given in the later section. The specific methods used to calculate m_{eq} and θ_{fa} are also described later.

The effective porosity ϕ_e was calculated by computing the percentage of void voxels after the local averaging procedure, in which macropores were obtained by "filling" nanopores. It corresponds to the ratio of "external" pore volume which contribute to mass transfer in clays if the assumptions are valid (Wong and Wang, 1997; Li et al., 2018). Table 1 indicates that the effective porosity decreases as particle density increases and varies somewhat with the structures even at the same density condition. It is especially small in the stacked structures (see the lower column of Fig.

Table 1 Various structural and pore characteristics for each metastable structure

Structure number	Diffusional tortuosity τ_{dz} (−)	Effective porosity ϕ_e (−)	Average orientation angle θ_{fa} (deg.)	Aspect ratio of particle clusters m_{eq} (−)
(I)	1.58	0.52	57.4	2.93
(II)	2.34	0.49	30.1	2.85
(III)	6.11	0.43	6.9	7.38
(IV)	1.71	0.42	54.6	2.95
(V)	2.18	0.39	35.7	3.17
(VI)	5.60	0.31	10.0	6.05
(VII)	1.75	0.38	52.5	2.57
(VIII)	2.08	0.36	40.8	3.15
(IX)	5.53	0.26	11.5	5.75
(X)	1.77	0.33	55.4	2.05
(XI)	2.26	0.31	40.8	2.65
(XII)	5.97	0.20	12.5	5.63
(XIII)	6.07	0.19	12.8	5.80
(XIV)	**6.85**	**0.20**	**12.6**	**5.71**

5), because many tiny pores present between platelet clusters. Estimating the effective porosity in actual clays is not easy because its definition is somewhat arbitrary. A few previous studies have attempted to determine it, such as Li et al. (2018), who reported that the effective porosity of natural smectite clays is approximately 0.25 to 0.6. The present results agree with their findings reasonably, supporting the validity of the local averaging procedure used here.

Next the diffusional tortuosity τ_{dz} which is shown in Table 1 is discussed. As is well-known, the tortuosity in clay layers shows the anisotropy (Keller et al., 2011). However only the tortuosity perpendicular to the platelet orientation (platelet compaction direction) was considered in this study. Under the calculation conditions, the tortuosity obtained from a random walk simulation is approximately from 1.5 to 6.0. As described earlier, the tortuosity is expressed as the ratio of flow path length to the system length geometrically. Compared these values with the observation of white part in Fig.5, the results shown here are intuitively agreement with the geometrical definition of tortuosity. For example, the geometrical tortuosity (pore length relative to system length) can be visually estimated as approximately 1 to 2 in platelet structure X (see white areas in Fig. 5), while the diffusional tortuosity $\tau_{dz} = 1.77$. Conversely, pores in platelet structure XII has substantial curvature, while the diffusional tortuosity $\tau_{dz} = 5.97$ in this structure. Although the discussion given here is qualitative, the results given here suggest that the diffusional tortuosity sufficiently represents the geometrical tortuosity which is based on the curvature of flow path.

The effects of macroscopic particle cluster structures on tortuosity are summarized as follows. In the upper and middle structures shown in Fig. 5, particles formed relatively large clusters with small aspect ratios. As a result, the void channels exhibit little curvature and the tortuosities are accordingly small. Conversely, the lower structures in Fig. 5 contain flattened particle clusters with large aspect ratios with substantially bent pore networks, resulting in significantly large tortuosities. The tortuosity in the platelet structures varied by several times even at the same density conditions. It suggests that particle structures do greatly influence transport properties in platelet particles like clay layers.

3.3 Macrostructures in Platelet Particles from Cluster Judgement

Pore networks are greatly affected by the macroscopic configurations of particles, and it is therefore vital to quantify such structural properties, as done by Li et al. (2018), who estimated aspect ratios and orientation angles to characterize clay structures. Therefore, these parameters are evaluated to quantitatively describe the structural characteristics. As it is not clear which particles belong to the same cluster within the platelet structures shown in Fig. 5, the size and shape of the clusters could not be explicitly determined. Accordingly, a cluster judgment was performed for all metastable structures, which allowed us to examine the parameters mentioned above.

Figure 6 shows the results of the cluster judgment and geometric structural properties for platelet structures X, XI and XII at a dry density of 0.66 Mg/m^3. Figs. 6 (a) and (b) indicates 3D snapshots and cross-sectional views of clustered platelets visualized by color. As shown in the figure, structures X and XI (upper and middle column) contain clusters which vary in size and orientation. In contrast, many flat clusters formed in the stacked structures XII (lower column), which had relatively uniform angles.

The aspect ratio (diameter/thickness) of each cluster was calculated to examine the size characteristics. Fig.6 (c) indicates histograms of the aspect ratios for the metastable structures. The results are only shown up to a value of 20. Structures X and XI (upper and middle column) had a large fraction of clusters with small aspect ratios, while few such clusters were found in structure XII (lower column), which had a relatively large number of clusters with large aspect ratios. Thus, entirely different cluster size features were observed even at the same density.

From the results of Fig.6(c), the averaged aspect ratio of each structures was calculated. Following the procedure of Daigle and Dugan (2011), the averaged aspect ratio m_{eq} is calculated as follows;

$$\frac{1}{m_{eq}} = \sum_{i=1}^{n} \frac{f_i}{m_i^2} \tag{14}$$

where f_i is the fraction of particles with an aspect ratio m_i. The averaged aspect ratios for each metastable structure are summarized in Table 1. Significant differences in cluster size can occur under the same density conditions. Compared among the platelet structures shown in Fig.6, the values of m_{eq} are 2.05 for structure X, 2.65 for structure XI, and 5.63 for structure XII, respectively. These are consistent with the aspect ratios of clusters observed visually from the cross-sectional views in Fig. 6 (b).

The platelet orientations are also evaluated by calculating the vertical orientation angles θ of platelets and then averaging them arithmetically. The histograms of orientation angles for structures X, XI, and XII are shown in Fig. 6 (d). As seen in the figure, structure X displays considerable variations in angle, but with a relatively uniform frequency with average angle θ_{fa} of 55.4 degree (see Table 1). Structure XI exhibits a hill-like distribution with an average angle of 40.8 degrees. In structure XII, approximately 70% of the platelets fell in the range of 10 to 20 degree with an average angle of 12.5 degrees. These results demonstrate a wide variety of angle distributions that can result even at a given density.

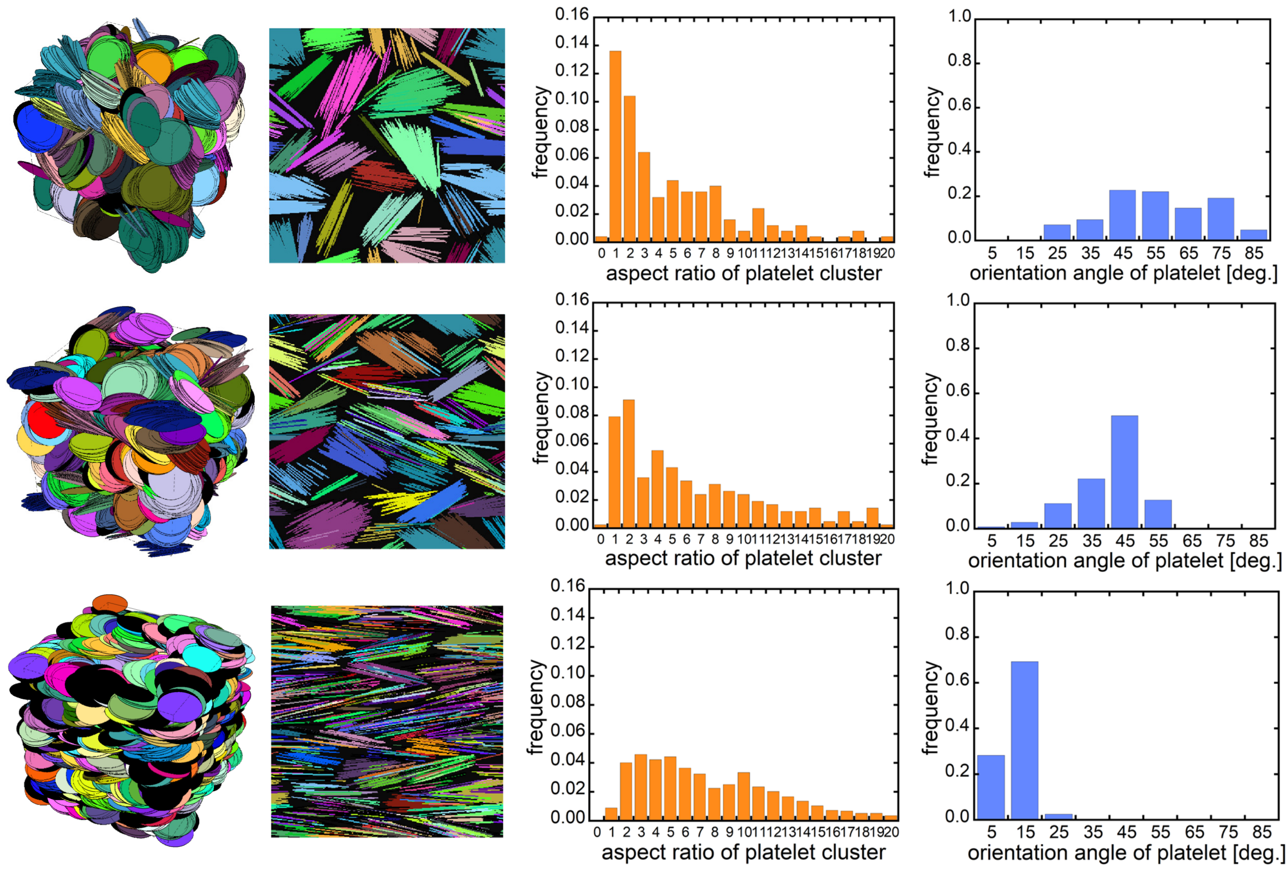

(a) 3D snapshots (b) cross-section (c) aspect ratio (d) orientation angle

Fig. 6 Results of cluster judgment and geometrical structural properties for various platelet structures at dry density ρ_d=0.66 Mg/m^3. Structural numbers are X (upper), XI (middle) and XII (lower), respectively.

In structures X and XI, which is shown in the upper and middle columns of Fig. 6, the averaged aspect ratio m_{eq} is approximately 2 to 3, and the average orientation angle θ_{fa} is approximately 50 degrees. These structures are visually similar to those of clay layers described in previous studies (e.g. Pusch, 1983). More quantitatively, Li et al. (2018) reported that the aspect ratios and orientation angles of particle clusters in smectite clays are approximately 2 to 3 and 30 to 60 degrees, respectively. The clustered structures described here are again comparable with their findings, although speculative, this comparison suggests that such structures may be found in clay layers in nature.

In structure XII, which is shown in the lower column of Fig. 6, the averaged aspect ratio m_{eq} are approximately 6 and the orientation angle θ_{fa} are around 10 degree. As noted earlier, for particle density above a certain level, the number of possible states is reduced and it is difficult for clustered structures to form, so that stacked structures may better represent clays that have experienced compaction.

3.4. Comparison with Tortuosity Model

The previous sections demonstrated that configurational properties significantly affect the tortuosity in platelet layers. In order to predict the tortuosity in platelet layers quantitatively, it is important to characterize such macroscopic structures. This section refers to the existing tortuosity models of particulate beds and describes the necessary parameters for tortuosity models of platelet layers.

As previously described, tortuosities may be defined in different ways. For isotropic particle layers such as spherical particulate bed, various models have been developed to represent each type of tortuosity. For examples, Millington (1959) theoretically systematized diffusional tortuosity and Koponen et al. (1996) modeled hydraulic tortuosity. Various other models have also been proposed from different perspectives (Weissberg, 1963; Boudreau, 1996; Ahmadi et al., 2011). In most studies, tortuosity in spherical particle bed has described as a function of porosity alone. In other words, the effects of macroscopic structures on tortuosity are expected to be small for isotropic particle beds.

In contrast, tortuosity in platelet layers cannot easily be described solely in terms of porosity because of the strong dependence on the macroscopic configuration. For example, Daigle and Dugan (2011) proposed a geometrical tortuosity model in platelet structures based on simple assumptions: they placed disk-shaped objects representing clay cluster at regularly spaced intervals and calculated the lengths of macropores geometrically. The resultant model is described as follows:

$$\tau_{gz} = 1 + \frac{\frac{8m}{9}\cos\left(\frac{\theta_1+\theta_2}{2}\right)+\sin\left(\frac{\theta_1+\theta_2}{2}\right)}{\frac{3\pi}{8(1-\phi)}-\frac{1}{2}} \tag{15}$$

where τ_{gz} is the geometrical tortuosity perpendicular to the platelet orientation, m is the aspect ratio of the particle cluster, ϕ is the porosity, and θ_1 and θ_2 represent the minimum and maximum orientation angles, respectively. They compared this model with the results of hydraulic tortuosity from lattice-Boltzmann simulations and confirmed the validity of their model. It means that they suggested a correspondence between the hydraulic and geometrical tortuosities. They also performed the geometric consideration of the tortuosity in polydispersed particle clusters using the averaged aspect ratio described in Eq.(14).

However, it is unclear whether the model in Eq.(15) can be used to express the tortuosity in more complicated structures. Therefore, the model validity was examined by comparing the diffusional tortuosity from a random walk analysis with that from geometrical tortuosity model, and additionally examined the influences of platelet structures to these tortuosities. Figure 7 shows comparisons between the present analyses and the model by Daigle and Dugan (2011). The black lines represent model results in which the averaged aspect ratio and orientation angle of each structure (see Table 1) was substituted into Eq. (15), and the red plots represent the tortuosity obtained from random walk analyses. As can be seen in Fig.7, the tortuosity increases gradually as porosity decreases and it varies greatly depending on the structure even at the same density condition. For example, as shown in Fig. 7 (d), the tortuosities in structure X ranged from approximately 1 to 4, while those in structure XII ranged from 1 to 9 even though the density conditions are the same. These variances are obviously caused by complicated dependency of the tortuosity on macrostructural characteristics.

Fig.7 also shows that the tortuosies from the model and the present analysis are generally in good agreement. However, the model results is slightly larger than that from the present analysis under some conditions. One of the reasons might be the angle averaging. Daigle and Dugan (2011) estimated

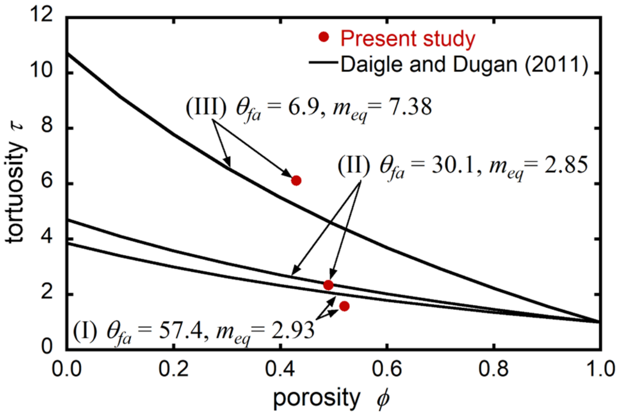

(a) ρ_d = 0.20 Mg/m^3

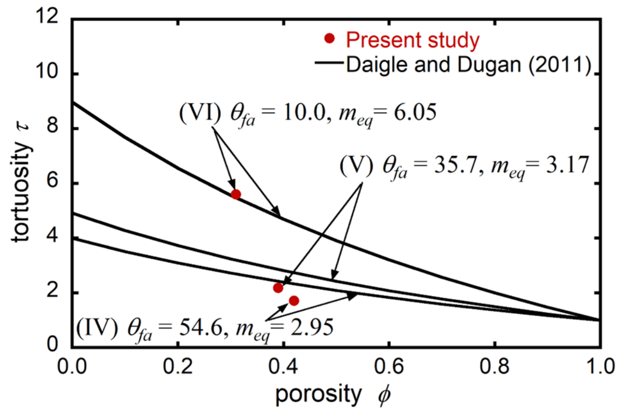

(b) ρ_d = 0.33 Mg/m^3

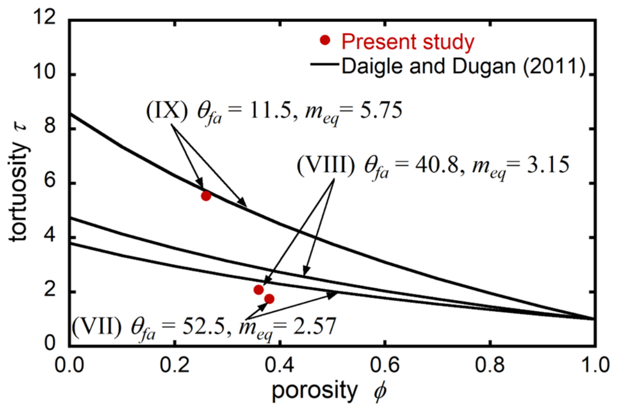

(c) ρ_d = 0.46 Mg/m^3

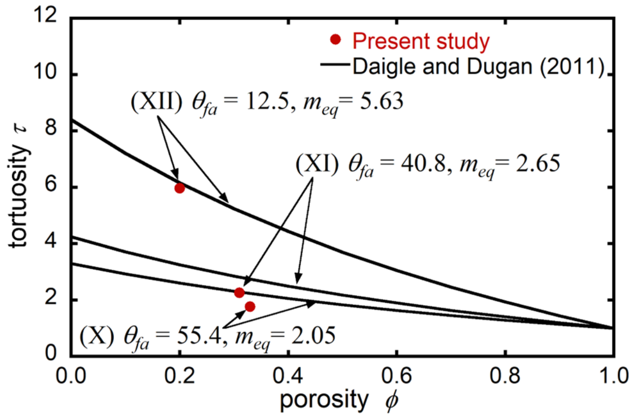

(d) ρ_d =0.66 Mg/m^3

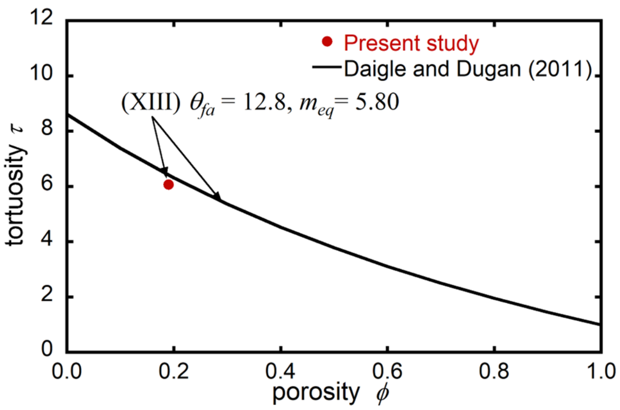

(e) ρ_d = 0.99 Mg/m^3

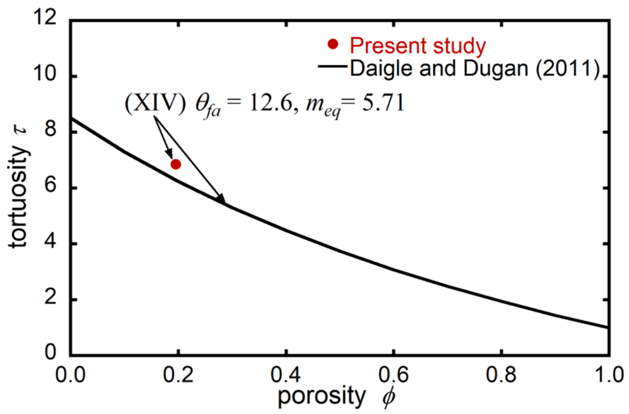

(f) ρ_d = 1.13 Mg/m^3

Fig. 7 Comparison of diffusional tortuosity and geometrical tortuosity model for each metastable structure.

the averaged angle from arithmetic average of minimum and maximum orientation angles, but actually the platelet angles have a wide range, as shown in Fig.6 (d). For example, the orientation angles ranges widely in clustered structures (see upper and middle columns of Fig. 6), suggesting that the above considerations may have produced differences between the model and the analysis. In contrast, stacked structures (see lower column of Fig. 6) exhibits only slight angle variations. In this case, the above effect is minor and the model results agree well with the results of random walk analysis. These results suggest as follows. First, the simple tortuosity model constructed by Daigle and Dugan (2011) could sufficiently evaluate the tortuosity in complex platelet structures for low to moderate density conditions. Their model expresses the tortuosity in both cluster and almost-stacked structures as shown in Fig.5. This implies that the model can be applied to more dense platelet layers with nematic structures, which is not shown here. Secondly, although the geometrical and diffusional tortuosities are defined differently, there might be a correspondence between them. Importantly, to estimate the tortuosity in platelet structures, it is vital to consider the macroscopic characteristics, such as the aspect ratio and the orientation angle of particle clusters.

3.5 Comparison with Diffusion Experiments

The diffusional tortuosity in the platelet structures was compared with the diffusion coefficient for actual clay layers. As described in Eq.(4), diffusional tortuosity is uniquely related to the diffusion coefficient of non-sorbing materials. Tritium (HTO) is used to experimentally determine diffusivity in clay layers without the influence of sorption effects. Bacle et al. (2016) summarized the relationship between dry density and diffusion coefficients from previous experiments in clay layers. Figure 8 shows the diffusion coefficients of tritium in the same direction as clay consolidation from their cited data (Choi and Oscarson, 1996; García-Gutiérrez et al., 2004; Sato and Suzuki, 2003; Suzuki et al., 2004; González-Sánchez et al., 2008; Glaus et al., 2010; Tachi and Yotsuji, 2014; Melkior, 2009; Sato et al., 1992; Kozaki et al., 1999; Nakashima, 2004; Nakashima and Mitsumori, 2005; Nakashima, 2001). The horizontal axis is dry density of clays and the vertical axis represents the ratio of the apparent diffusion coefficient D_a to the self-diffusion coefficient D_0.

Experimental results in Fig. 8 indicate the complicated density dependency of the diffusion coefficient. At low density (ρ_d < 0.6 Mg/m^3), the diffusion coefficient monotonically decreases with increasing density. At moderate density (ρ_d > 0.6 Mg/m^3), the diffusion coefficient displays significant variations of around one order of magnitude for a given density. Bacle et al. (2016) numerically analyzed diffusion coefficients in clay layers in comparison with experimental results at various density conditions. They applied the Gay-Berne potential to thick plates and computed the results for high-density conditions. However, their structural analysis allowed for overlap between particles, and it is difficult to determine whether the macropores resulting from the excluded volume effect associated with the clustering of platelet particles were appropriately modeled.

The diffusional tortuosity in macropores formed by the excluded volume effect was compared with existing experimental results, similar to Bacle et al. (2016). The colored plots in Fig. 8 indicate the diffusion coefficient converted from the tortuosity of structures I to XIV obtained from a random walk analyses using Eq. (4). It should be noted that, all structures do not represent the actual structure of clay layers, because these are parametrically prepared in the analysis. At low density conditions (ρ_d = 0.20–0.46 Mg/m^3) shown in Fig. 8, the diffusion coefficient in stacked structures (structures III, VI and IX) differed strongly from the experimental results, while those for clustered structures (structures I, II, IV, V, VII and VIII) were in good agreement with the experiments.

As indicated in Table1, these clustered structures have the aspect ratio m_{eq} of around 2 to 4 and an orientation angle θ_{fa} of 30 to 60 degree. These values are relatively consistent with smectite structures reported by Li et al. (2018). At high density (ρ_d =0.66–1.13 Mg/m^3), the diffusion coefficient in stacked structures (structures XII, XIII and XIV) approaches those of the experiments. Such agreements indicate that the actual clay particles may have nematic structures under high density conditions that would increase the number of possible particle states.

These results suggest that the density dependence of the diffusivity in clay layers would result from the diversity of particle structures with anisotropic shapes. At low density conditions, only slight variations in the diffusion coefficient from the experiments occur, which tend to decrease monotonically. In this density range, the values are quantitatively consistent with the diffusion coefficients in clustered structures, such as those found in common clay layers. However, at moderate density conditions, the significant variations in the diffusion coefficient are quantitatively consistent with the tortuosity in clustered structures at the upper limit and with the tortuosity in stacked structures at the lower limit. As mentioned earlier, clay structures depend on the formation process and conditions, therefore various internal structures are presumed to have formed under these density conditions. The diffusion coefficients are expected to convert to the values found in nematic structures at high density conditions. This result is likely due to the excluded volume effect, which limits the number of possible platelet states. Accordingly, the macroscopic particle structure significantly influenced the pore characteristics, particularly the tortuosity which directly relates to the diffusional transport. As mentioned above, the present analysis was performed only for low to moderate density conditions. Although the results shown here do not cover all of the dry densities of clays generallyconsidered, they capture the discontinuous changes in tortuosity (diffusion coefficient) that occur at moderate density conditions. This could be a possible scenario explaining the complicated

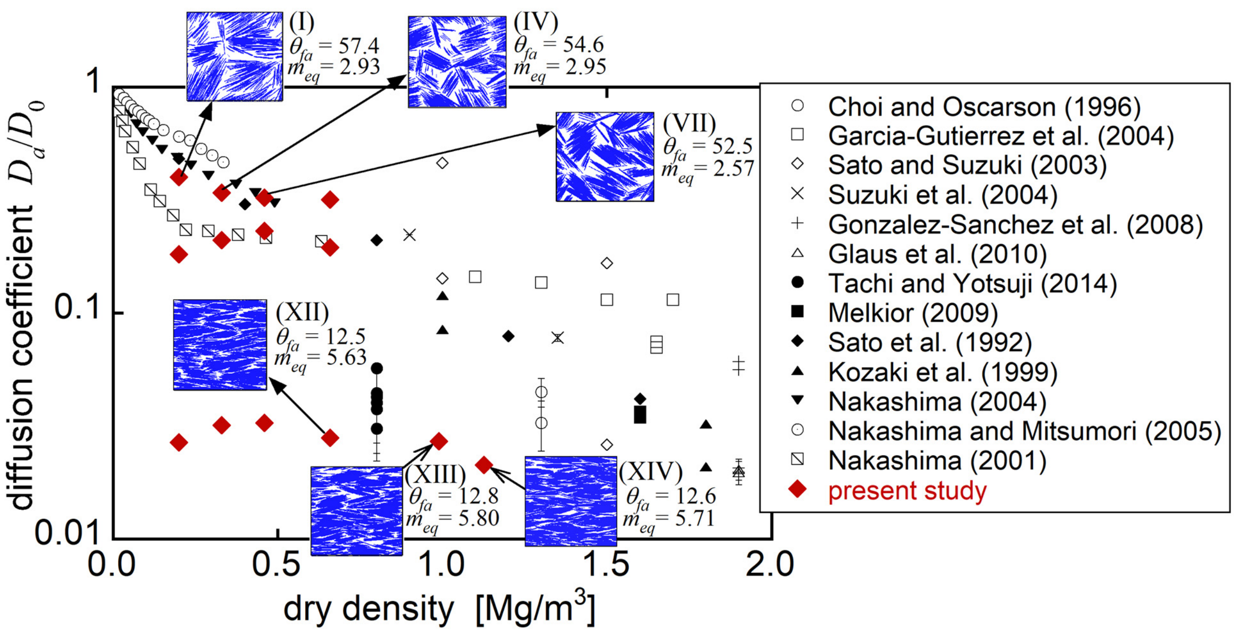

Fig. 8 Comparison of diffusion coefficients from random walk analysis and previous diffusion experiments in smectite type clays.

diffusivity in clay layers.

4. Conclusion

For fundamental understanding of pore characteristics in clay layers composed of montmorillonite particles, the relationship between the tortuosity which represents the sinuosity and complexity of pores and macroscopic structures of platelet particles was examined. Monte Carlo analyses of platelet structures were performed using various initial configurations to investigate how macroscopic particle structures influence pore networks. Various metastable platelet structures containing particle clusters were computed for low to moderate density conditions. The pore characteristics were examined by extracting only those macropores that would contribute to mass transport.

A random walk analysis was also performed on the macropores to estimate the diffusional tortuosity in the platelet compaction direction. The results indicate that the structural characteristics of particles, such as the size and angle of platelet clusters, significantly influence the tortuosity. These results suggest that pore networks in platelet structures may vary depending on the internal configuration. Therefore, it is important to fully characterize the macroscopic structure of particles when evaluating mass transport properties such as permeability and diffusion.

The effective porosity, orientation angles, and aspect ratios of particle clusters were quantitatively estimated for each platelet structure. The diffusional tortuosity obtained from random walk analyses was compared with an existing geometrical tortuosity model. The results indicate a general agreement between the previous model and the present analysis under specific density conditions, supporting the validity of the model. This finding indicates a correspondence between diffusional and geometrical tortuosities, which are differently defined. Based on these results, the macroscopic structural characteristics are essential parameters for evaluation of tortuosity in platelet structures.

The obtained tortuosity from random walk analyses was converted into the diffusion coefficient and compared with those of previous diffusion experiments in clay layers. Good agreement was observed between the analytical and experimental results at structures with specific aspect ratio and orientation angle of clusters for low to moderate density conditions. The structural consistency differs depending on the density condition, indicating that complex diffusivity in clay layers may result from the diversity of particle structures.

Acknowledgements

This study was carried out under a contract with the Ministry of Economy, Trade and Industry (METI) as part of its R&D supporting program titled "Advanced technology development for geological disposal of TRU waste (FY2020) (JPJ007597)". We would like to thank Dr. H. Satoh and I. Kobayashi for many helpful comments and valuable discussions.

References

Patil, S. B. and Chore, H. S., Contaminant transport through porous media: An overview of experimental and numerical studies, *Adv. Environ. Res.*, **3**-1 (2014), 45-69.

Åkesson, M., Kristensson, O., Börgesson, L. and Dueck, A., THM modelling of buffer, backfill and other system components, SKB TR, **10**-44 (2010).

Carman, P. C., Fluid flow through granular beds, *Trans. Inst. Chem. Eng.*, **15** (1937), 150-156.

Holzer, L., Wiedenmann, D., Münch, B., Keller, L., Prestat, M., Gasser, P., Robertson, I. and Grobéty, B., The influence of constrictivity on the effective transport properties of porous layers in electrolysis and fuel cells, *J. Mater. Sci.*, **48** (2013), 2934-2952.

Keller, L. M., Hilger, A. and Manke, I., Impact of sand content on solute diffusion in Opalinus Clay, *Appl. Clay Sci.*, **112-113** (2015), 134-142.

Clennell, M. B., Tortuosity: a guide through the maze. *Geol. Soc. Lond., Spec. Publ.*, **122** (1997), 299–344.

Ghanbarian, B., Hunt, A. G., Ewing, R. P. and Sahimi, M., Tortuosity in porous media: A critical review, *Soil. Sci. Soc. Am. J.*, **20** (2013), 1461-1477.

Fu, J., Thomas, H.R. and Li, C., Tortuosity of porous media: Image analysis and physical simulation, *Earth Sci. Rev.*, **212** (2021), 103439, 1-30.

Milllington, R. J., Gas diffusion in porous media, *Sci.*, **130** (1959), 100-102

Weissberg, H. L., Effective diffusion coefficient in porous media, *J. Appl. Phys.*, **34** (1963), 2636-2639.

Boudreau, B. P., The diffusive tortuosity of fine-grained unlithified sediments, *Geochim. Cosmochim. Acta.*, **60** (1996), 3139-3142.

Koponen, A., Kataja, M. and Timonen, J., Tortuous flow in porous media, *Phys. Rev. E*, **54** (1996), 406-410.

Ahmadi, M. M., Mohammadi, S. and Hayati, A. N., Analytical derivation of tortuosity and permeability of monosized spheres: A volume averaging approach, *Phys. Rev. E*, **83** (2011), 026312, 1-8.

Daigle, H. and Dugan, B., Permeability anisotropy and fabric development: A mechanistic explanation, *Water Resour. Res.*, **47** (2011), W12517.

Dijikstra, M., Hansen, J.-P. and Madden, P. A., Statistical model for the structural and gelation of smectite clay suspensions, *Phys. Rev. E*, **55** (1996), 3044-3053.
Keller, L. M., Holzer, L., Wepf, R. and Gasser, P., 3D geometry and topology of pore pathways in Opalinus clay: Implications for mass transport, *Appl. Clay Sci.*, **52** (2011), 85-95.
Wong, R. C. K. and Wang, E. Z., Three-dimensional anisotropic swelling model for clay shale-A fabric approach, *Int. J. Rock Mech. Min. Sci.*, **34** (1997), 187-198.
Olsen, H. W., Hydraulic flow through saturated clays, *Clays Clay Miner.*, **9** (1960), 131-161.
Hong, B., Li, X., Wang, L., Wang, L., Xue, Q. and Meng, J., Using the effective void ratio and specific surface area in the Kozeny-Carman equation to predict the hydraulic conductivity of Loess, *Water*, **12**-24 (2020), W12010024.
Bacle, P., Dufrêche, J.-F., Rotenberg, B., Bourg, I. C. and Marry, V., Modeling the transport of water and ionic tracers in a micrometric clay sample, *Appl. Clay Sci.*, **123** (2016), 18-28.
Boţan, A., Rotenberg, B., Marry, V., Turq, P. and Noetinger, B., Hydrodynamics in clay nanopores, *J. Phys. Chem. C*, **115** (2011), 16109-16115.
Li, B., Wong, R. C. K. and Heidari, S., A modified Kozeny-Carman model for estimating anisotropic permeability of soft mudrocks, *Mar. Pet. Geol.*, **98** (2018), 356-368.
Adams, A. L., Germaine, J. T., Flemings, P. B. and Day-Stirrat, R. J., Stress induced permeability anisotropy of resedimented Boston Blue clay, *Water Resour. Res.*, **49** (2013), 6561-6571.
Terada, K., Tani, A., Harada, S., Satoh, H. and Hayashi, D., Monte Carlo analysis of montmorillonite particle structures and modeling of dissolution rate reduction, *Mat. Res. Express*, **6** (2018), 035514
Singh, P. N. and Wallender, W. W., Effects of adsorbed water layer in predicting saturated hydraulic conductivity for clays with Kozeny-Carman equation, *J. Geotech. Geoenviron. Eng.*, **134**-6 (2008), 829-836.
Satterfield, C. N. and Sherwood, T.K., *The role of diffusion in catalysis*, (1963), Addison-Wesley, Reading, MA.
Tye, F.L., Tortuosity, *J. Power Sources*, **9** (1983), 89-100.
Adler, P. M., *Porous media: Geometry and transports*, (1992), Butterworth–Heinemann, Stoneham, MA.
Vervoort, R.W. and S.R. Cattle, Linking hydraulic conductivity and tortuosityparameters to pore space geometry and pore-size distribution, *J. Hydrol.*, **272** (2003), 36-49.
García-Gutiérrez, M., Cormenzana, J. L., Missana, T. and Mingarro, M., Diffusion coefficients and accessible porosity for HTO and ^{36}Cl in compacted FEBEX bentonite, *Appl. Clay. Sci.*, **26** (2004), 65-73.
Gautam, R., Anisotropy in deformations and hydraulic properties of Colorado shale. PhD thesis, Department of Civil Engineering, University of Calgary, (2004).
Chalindar, S., Charlier, R., Collin, F., Dizier, A., François, B., Fokkens, J., Garitte, B., Gens, A., Chen, G., Hart, J., Laloui, L. and Sillen, X., Thermal impact on the damaged zone around a radioactive waste disposal in clay host rocks, deliverable 13: In situ heating test ATLAS in Mol, *TIMODAZ project. EUROPEAN COMMISION*, (2010).
Schneider, J., Flemings, P.B., Day-Stirrat, R.J. and Germaine, J.T., Insights into porescale controls on mudstone permeability through resedimentation experiments, *Geology*, **39** (2011), 1011–1014.
Wouterse, A., Williams, S. R. and Philipse, A. P., Effect of particle shape on the density and microstructure of random packings, *J. Phys.*: *Condens. Matter*, **19** (2007), 406215.
Pusch, R., Stability of bentonite gels in crystalline rock – Physical aspects, SKBF/KBS Technical Report, **84**-04 (1983).
Choi, J.-W. and Oscarson, D. W., Diffusive transport through compacted Na- and Ca-bentonite, *J. Contam. Hydrol.*, **22** (1996), 189-202.
Sato, H. and Suzuki, S., Fundamental study on the effect of an orientation of clay particles on diffusion pathway in compacted bentonite, *Appl. Clay. Sci.*, **23** (2003), 51-60.
Suzuki, S., Sato, H., Ishidera, T. and Fujii, N., Study on anisotropy of effective diffusion

coefficient and activation energy for deuterated water in compacted sodium bentonite, *J. Contam. Hydrol*, **68** (2004), 23-37.

González-Sánchez, F., Van Loon, L. R., Gimmi, T., Jakob, A., Glaus, M. A. and Diamond, L. W., Self-diffusion of water and its dependence on temperature and ionic strength in highly compacted montmorillonite, illite and kaolinite, *Appl. Geochemistry*, **23** (2008), 3840-3851.

Glaus, M. A., Frick, S., Rossé, R. and Van Loon, L. R., Comparative study of tracer diffusion of HTO, $^{22}Na^{+}$ and $^{36}Cl^{-}$ in compacted kaolinite, illite and montmorillonite, *Geochim. Cosmochim. Acta.*, **74** (2010), 1999-2010.

Tachi, Y. and Yotsuji, K., Diffusion and sorption of Cs^{+}, Na^{+}, I- and HTO in compacted sodium montmorillonite as a function of porewater salinity: Integrated sorption and diffusion model, *Geochim. Cosmochim. Acta.*, **132** (2014), 75-93.

Melkior, T., Gaucher, E. C., Brouard, C., Yahiaoui, S., Thoby, D., Clinard, C., Ferrage, E., Guyonnet, D., Tournassat, C. and Coelho, D., Na^{+} and HTO diffusion in compacted bentonite: Effective surface chemistry and related texture, *J. Hydrol*, **370** (2009), 9-20.

Sato, H., Ashida, T., Kohara, Y., Yui, M. and Sasaki, N., Effect of dry density of some radionuclides in compacted sodium bentonite, *J. Nucl. Sci. Technol.*, **29**-9 (1992), 873-882.

Kozaki, T., Sato, Y., Nakajima, M., Kato, H., Sato, S. and Ohashi, H., Effect of particle size on the diffusion behavior of some radionuclides in compacted bentonite, *J. Nucl. Mater.*, **270** (1999), 265-272.

Nakashima, Y., Nuclear magnetic resonance properties of water rich gels of Kunigel-V1 bentonite, *J. Nucl. Sci. Technol.*, **41**-10 (2004), 981-992.

Nakashima, Y. and Mitsumori, F., H_2O self-difussion restricted by clay platelets with immobilized bound H_2O layers: PGSE NMR study of water-rich saponite gels, *Appl. Clay Sci.*, **28** (2005), 209-221.

Nakashima, Y., Pulsed filed gradient proton NMR study of the self-diffusion of H_2O in montmorillonite gel: Effects of temperature and water fraction, *Am. Mineral.*, **85** (2001), 132-138.

617